



# ACOUSTICS 2012

## Investigation on streaming sources in thermoacoustic prime mover

R. Paridaens, S. Koudri and F. Jebali Jerbi

LIMSI-CNRS, BP 133, 91403 Orsay, France, Metropolitan  
richard.paridaens@imelavi.fr

Nonlinear propagation of high amplitude acoustic waves causes the appearance of secondary flow. This flow called acoustic streaming is superimposed to the oscillating flow. In thermoacoustic devices, the streaming is the source of an important energy dissipation and therefore a significant decrease of efficiency. In this paper, the streaming velocity is studied in an acoustic device and a comparison between theoretical and experimental results is made. This paper also deals with the phenomena at the origin of the streaming and the contribution of each phenomenon is quantified versus the channel diameter.

## 1 Introduction

Thermoacoustic devices either prime mover, heat engines or refrigerators are not known for their high efficiency. Even though these systems have many advantages regarding environmental constraints, they are not yet used in the industrial applications. Energy conversion efficiency improvement of thermoacoustic systems is now in the priority of the thermoacoustic community. One of the reasons of the relative low efficiencies is in the physical understanding which is not well achieved.

The high mean pressure amplitude in these machines, necessary for their functioning are responsible of the appearance of steady mass flow of second order. Usually called streaming, it is superimposed to the first order oscillating mass flow. These dissipating energy phenomena come from the nonlinear propagation. From energy consideration and despite their low level, these second order phenomena involve heat transfer to the wall which is undesirable loss mechanism. As the acoustic streaming has been identified as an important source of energy dissipation in thermoacoustic devices [1, 2], a better understanding of this phenomenon is necessary to improve their efficiency. This phenomenon which is a quite old topic is still widely investigated experimentally and theoretically. Many studies on acoustic streaming have been conducted for the last 20 years. However, the different phenomena at the origin of the acoustic streaming have not been quantified. Lighthill gave an explication of the acoustic streaming generation by introducing the Reynolds stress tensor for acoustic waves [3]. Olson and Swift explained the streaming generation by the spatial variation of the viscosity [4]. Bailliet and al. has quantified the influence of the viscosity on the streaming generation [5].

The phenomena at the origin of the acoustic streaming are physically described and quantified in this paper. The contribution of the streaming sources is quantified versus geometrical parameters of the acoustic device.

## 2 Theory

In thermoacoustic device, the fluid is governed by conservation laws. In an Eulerian coordinate system attached to the resonator, the equations for mass, momentum and energy lead to [6]:

$$\frac{\partial \rho}{\partial t} + \frac{\partial(\rho u_i)}{\partial x_i} = 0 \quad (1)$$

$$\rho \frac{\partial u_i}{\partial t} + \rho u_k \frac{\partial(u_i)}{\partial x_k} = -\frac{\partial p}{\partial x_i} + \frac{\partial \sigma_{ik}}{\partial x_k} \quad (2)$$

with:

$$\sigma_{ik} = \mu \left( \frac{\partial u_i}{\partial x_k} + \frac{\partial u_k}{\partial x_i} - \frac{2}{3} \delta_{ik} \frac{\partial u_l}{\partial x_l} \right) + \mu_B \delta_{ik} \frac{\partial u_l}{\partial x_l} \quad (3)$$

where  $\rho$  and  $p$  are respectively the density and the pressure of the fluid.  $u_i$  is the component of the particle's velocity.  $\sigma_{ik}$  is the viscous stress tensor.  $\mu$  and  $\mu_B$  are respectively the shear viscosity and the bulk viscosity.  $c_p$  is the specific heat at constant pressure and  $\delta_{ik}$  the Kronecker delta.

Assumptions are made in order to study nonlinear effects in thermoacoustic devices. A secondary flow is assumed to be superimposed to the primary oscillating flow. Time and space dependent variables can be written in a manner to take into account variables in the absence of oscillations ( $\rho_0$ ,  $p_0$ ), acoustic variables ( $\rho'$ ,  $p'$ ,  $\vec{v}'$ ) and secondary flow variables ( $\rho_m$ ,  $p_m$ ,  $\vec{v}_m$ ):

$$\rho = \rho_0 + \rho' + \rho_m \quad p = p_0 + p' + p_m \quad \vec{v} = \vec{v}' + \vec{v}_m \quad (4)$$

Generally, the transversal dimension in thermoacoustic devices is much smaller than the longitudinal one. By a dimensional analysis of equations (1) and (2), the total pressure can be considered as depending only on the  $x$  component [6]. The acoustic Mach number is assumed much smaller than 1. Streaming is assumed stationary and the Mach number associated to the secondary flow is less than 0.3. Therefore, the secondary flow is expected to be incompressible. The Reynolds number of the streaming is significantly less than 1, so that the advection term is neglectable compared to the viscosity term. Thus the secondary flow is called slow streaming. In this paper, the investigation focuses on the Rayleigh streaming and the mass flow through any cross section is zero in the steady-state operation. Under these assumptions, the equations governing the streaming are written [5]:

$$\rho_0 \left[ \frac{\partial u_m}{\partial x} + \frac{\partial v_m}{\partial y} \right] = S \quad (5)$$

$$0 = -\frac{\partial p_m}{\partial x} + \mu_0 \frac{\partial^2 u_m}{\partial y^2} + F_R + F_\mu \quad (6)$$

$$\frac{\partial p_m}{\partial y} \approx 0 \quad (7)$$

Where:

$$S = - \left[ \frac{\partial \overline{\rho_1 u_1}}{\partial x} + \frac{\partial \overline{\rho_1 v_1}}{\partial y} \right] \quad (8)$$

and

$$F_R = - \left[ \frac{\partial \overline{\rho_0 u_1 u_1}}{\partial x} + \frac{\partial \overline{\rho_0 v_1 u_1}}{\partial y} \right] \quad (9)$$

$$F_\mu = \frac{\partial}{\partial y} \left[ \overline{\mu_1 \frac{\partial u_1}{\partial y}} \right] \quad (10)$$

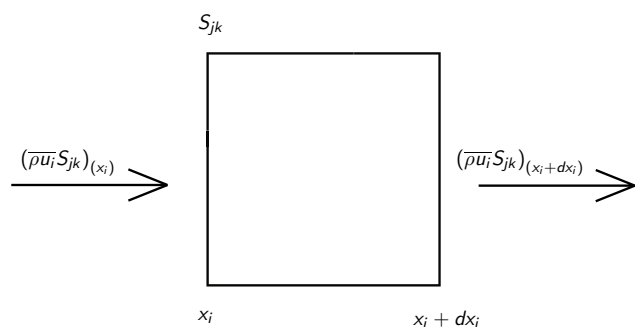
The equations (5) and (7) are respectively the mass and momentum conservation equations governing the streaming. The energy equation does not govern the acoustic streaming.  $\overline{\quad}$  indicates the average time of the quantity inside.  $u_m$  et  $v_m$  are respectively the axial and the transversal velocity of the acoustic streaming.

$p_m$  is the pression generated by the streaming.  $u_1$  et  $v_1$  are respectively the axial and the transversale acoustic velocity.  $\mu_0$  is the shear viscosity and  $\mu_1$  the variation in viscosity provided by the acoustic wave.  $\rho_0$  is the density of the fluid and  $\rho_1$  is density variation added by the acoustic wave.  $F_R$  et  $F_\mu$  are the acoustic streaming source terms due respectively to the spatial variation of the Reynolds stress tensor and viscous stress tensor. They are only governed by acoustic field.  $S$  represents a volume flow rate.

The term  $S$  is a mass flow induced by the propagation of the acoustic wave. In order to better understand the meaning of this term, the average flow is assumed to be zero. The density and the velocity are expressed as follow:

$$\rho = \rho_0 + \rho_1 \quad u = u_1 \quad (11)$$

The mass flow accumulated inside an elementary vol-



ume  $d\tau = dx_i dx_j dx_k$  is:

$$d\dot{M} = [\overline{\rho_1 u_i}(x_i) - \overline{\rho_1 u_i}(x_i + dx_i)] S_{jk} = -\frac{\partial \overline{\rho_1 u_i}}{\partial x_i} S_{jk} dx_i \quad (12)$$

$S_{jk} = dx_j dx_k |_{j,k \neq i}$  is an elementary surface of the volume  $d\tau$ . The mass accumulation per unit of volume and time can be written as

$$d\dot{m} = \frac{d\dot{M}}{d\tau} = -\frac{\partial \overline{\rho_1 u_i}}{\partial x_i} = S \quad (13)$$

Without an average flow,  $S$  would represent the mass flow accumulation per unit of volume. As there is no accumulation, the mass is evacuated by the acoustic streaming.

In sound waves, Reynolds stress tensor is defined [3]:

$$\overline{\rho_0 u_{1i} u_{1j}} \quad (14)$$

$u_{1i}$  is the  $i$ -component of the acoustic velocity. The spatial variation of the Reynolds stress tensor causes a net force per unit volume  $F_{Rj}$

$$F_{Rj} = -\frac{\partial (\overline{\rho_0 u_{1i} u_{1j}})}{\partial x_i} \quad (15)$$

The term  $F_R$  in equation (9) is the  $x$ -component of  $F_{Rj}$ . It is composed of two terms

$$F_{Ru} = -\frac{\partial \overline{\rho_0 u_{1i} u_{1i}}}{\partial x} \quad (16)$$

and

$$F_{Rv} = -\frac{\partial \overline{\rho_0 v_{1i} u_{1i}}}{\partial y} \quad (17)$$

The spatial variation of the viscous stress tensor generates a volumic force:

$$F_{\mu j} = \frac{\partial \overline{\sigma_{ik}}}{\partial x_k} \quad (18)$$

The average time of the force is non-zero because of the viscosity time-dependent in an Eulerian coordinate.  $F_\mu$  is the  $x$ -component of the average force  $F_{\mu j}$ .

The resolution of the equations (5-10) at the second order gives the expression of the axial streaming velocity [5]:

$$u_m = \phi_1 + \phi_2 + \phi_3 + \phi_4 \quad (19)$$

$$\phi_1 = \frac{3}{4\rho_0} (\eta^2 - 1) \int_{-1}^1 \overline{\rho_1 u_1} d\eta \quad (20)$$

$$\begin{aligned} \phi_2 = \frac{R^2}{\mu_0} \left[ \int_1^\eta \int_0^{\eta'} \frac{\partial (\overline{\rho_0 u_1 u_1})}{\partial x} d\eta'' d\eta' \right. \\ \left. - \frac{3}{4}(1 - \eta^2) \int_{-1}^1 \int_1^\eta \int_0^{\eta'} \frac{\partial (\overline{\rho_0 u_1 u_1})}{\partial x} d\eta'' d\eta' d\eta \right] \quad (21) \end{aligned}$$

$$\phi_3 = \frac{R}{\nu_0} \left[ \int_1^\eta \overline{u_1 v_1} d\eta' - \frac{3}{4}(1 - \eta^2) \int_{-1}^1 \int_1^\eta \overline{u_1 v_1} d\eta' d\eta \right] \quad (22)$$

$$\begin{aligned} \phi_4 = -\frac{\beta}{T_0} \left[ \int_1^\eta \left( T_1 \frac{\partial u_1}{\partial \eta} \right) d\eta' \right. \\ \left. - \frac{3}{4}(1 - \eta^2) \int_{-1}^1 \int_1^\eta T_1 \frac{\partial u_1}{\partial \eta} d\eta' d\eta \right] \quad (23) \end{aligned}$$

The equation (19) shows that the axial streaming velocity is made of four contributions.  $\phi_1$ ,  $\phi_2$ ,  $\phi_3$  and  $\phi_4$  are respectively the contribution of the term  $S$ ,  $F_{Ru}$ ,  $F_{Rv}$ ,  $F_\mu$  to the axial streaming velocity.  $\eta = y/R$  is the normalised transversal dimension.

### 3 Experimental setup

The device consists of a loudspeaker connected to a duct by a tapered tube (figure 1). The loudspeaker can provide a power of 300W and the particle velocity in the tube can reach a velocity higher than 5 m/s. The diameter of the membrane is 238 mm. The tapered tube is 600 mm long and it has an angle of 9.2 degrees. The duct is a 2m long cylinder with a 80 mm diameter circular section. The duct is transparent allowing measurements by Laser Doppler Velocimetry (LDV). It is closed at the extremity. The loudspeaker operates at 127 Hz a resonance frequency of the system. Three microphones are located on the duct allowing the measurement of the acoustic pressure. In the duct, measurements of the acoustic velocity and the streaming velocity are performed. The LDV system used a 660-nm wavelength laser. Its deliver power is 35 mW. Wood smoke is introduced into the device to visualize the flow. Measurements of the flow velocity are performed along the duct for  $y = 0$ . The measurement of the streaming velocity is obtained by an analyzed of 50 000 data of the flow velocity. The procedure used is described by Moreau and al. [7].

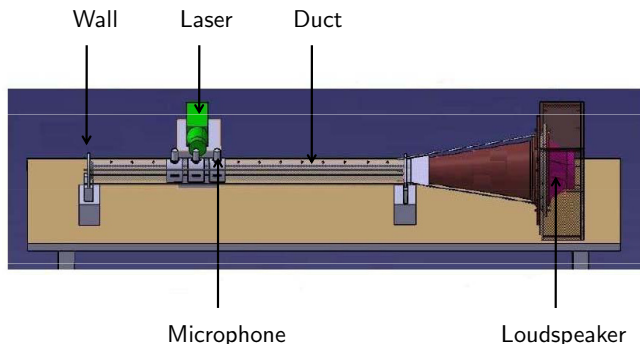


Figure 1: Experimental setup

## 4 Results

As acoustic streaming is generated by acoustic field (5-10), investigations are made on the first order before investigating the second order. The experimental data are compared to the theoretical results. Once satisfactory agreements are obtained, a comparison between theoretical and experimental streaming velocity is undertaken. After the validation of the acoustic and streaming fields, the investigation could be carried further: the streaming sources are quantified in function of the channel diameter for a standing wave.

The acoustic pressure along the duct for different supply voltages of the speaker is represented on the figure 2. The experimental and theoretical results are compared. At  $x=1.48\text{m}$  and at  $x=1.88\text{m}$ , the relative errors are respectively less than 4% and 45%. At  $x=1.68\text{m}$ , the measures were used as inputs for the theoretical model. Two pressure nodes are located at the position  $x=0.49\text{m}$  et  $x=1.95\text{m}$ . The variation of the magnitude from 0 to 0.6 m can be explained by the variation of the transversal section due to the tapered tube.

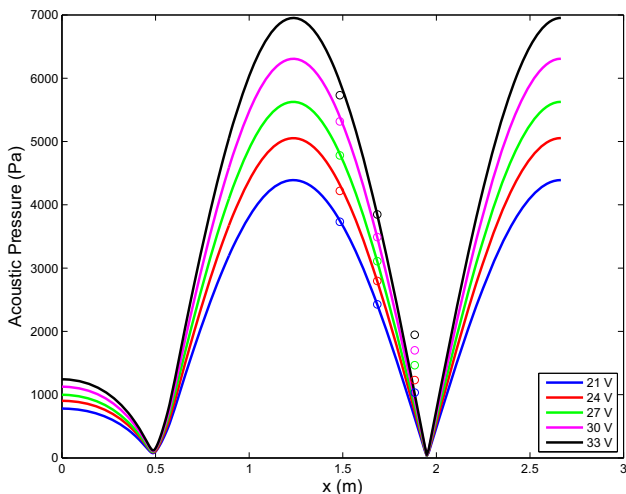
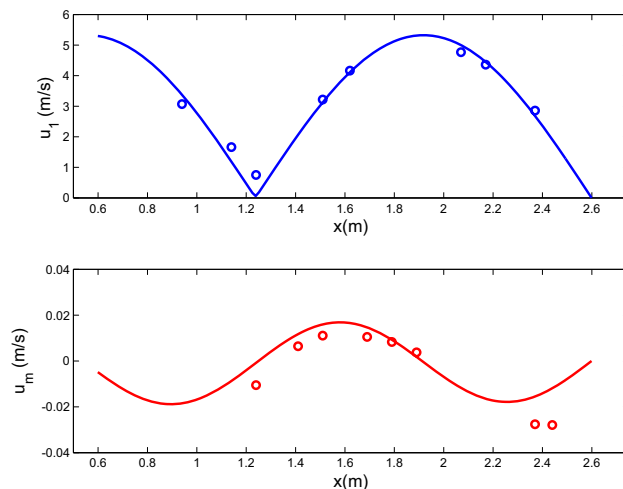


Figure 2: Acoustic pressure distribution for different supply voltages

Figure 3 represents the distribution of the acoustic and streaming velocity along the the duct for  $U=33\text{V}$ . Two velocity nodes are located at the position  $x=1.24\text{m}$  and  $x=2.6\text{m}$ . The node at the position  $x=2.6\text{m}$  is due to the condition of non penetration into the wall. At the position  $x=1.95\text{m}$ , there is a velocity antinode and also

a pressure node (figure 2). This correspondence between the velocity antinode and the pressure node is characteristic of a standing wave. For the acoustic and the streaming velocity, the theoretical results fit with the experimental ones. Regardless of the measurement near the velocity node, the relative error between the theoretical and experimental results for the acoustic velocity for  $x$  varying from 0.6 m to 1.3 m is less than 12%. For 1.3 m to 2.6 m, the relative error is less than 6%. The edge effect due to the connection of the tapered tube and the duct can explain the difference between the errors. The position of acoustic velocity nodes and antinodes correspond to the position of streaming velocity nodes. The large discrepancy between experimental and theoretical values at the position  $x=2.37\text{m}$  and  $2.44\text{m}$  can be explained by the end wall effect.

Figure 3: Distribution of the acoustic and streaming velocity along the the duct for  $U=33\text{V}$ 

The distribution of the different contributions to the acoustic streaming velocity at  $y=0$  is represented in figure 4. The contributions of  $S$ ,  $F_{Ru}$ ,  $F_{Rv}$ ,  $F_{\mu}$  to the axial streaming are respectively represented by  $T_1$ ,  $T_2$ ,  $T_3$ ,  $T_4$ . They are calculated as followed

$$T_i = \frac{|\phi_i|}{|\phi_1| + |\phi_2| + |\phi_3| + |\phi_4|} \quad (24)$$

The studied system has a ratio of  $R/\delta_\nu = 4060$ . According to the figure 4, the contributions  $T_i$  do not depend on the  $x$  component. Different values of  $R/\delta_\nu$  had been investigated. It seems that for standing waves when the magnitude of the wave does not depend on the  $x$  component, the contributions do not depend either on the  $x$  component. The contributions are also independent of the magnitude of the wave. In this case,  $T_1$ ,  $T_2$ ,  $T_3$  and  $T_4$  have respectively a contribution of 4%, 50%, 38% and 8%.

Subsequently, still in case of a standing wave, the investigation is performed on the variation of the ratio  $R/\delta_\nu$  for air, nitrogen and azote.

Figure 5 represents  $T_1$  at the position  $y=0$  in function of  $R/\delta_\nu$ . Whatever the type of gas, the curves have a similar form. When  $R/\delta_\nu$  tends to zero,  $T_1$  tends to 100% for the air, nitrogen and helium. When  $R/\delta_\nu$  tends to infinity,  $T_1$  tends to 0.4% for air and nitrogen and

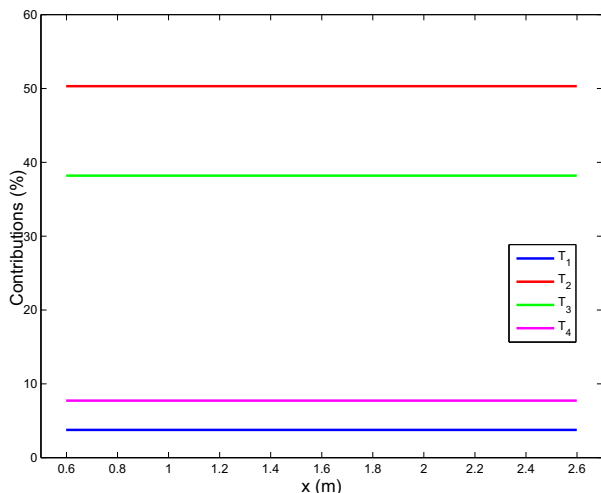


Figure 4: Different contributions to the acoustic streaming velocity at  $y=0$

to 0.5% for helium. Two specific values are observed. For  $R/\delta_\nu = 3.8$  and  $7.4$ ,  $T_1$  reaches respectively a local minimum and a local maximum. The local minima are 20% for air and nitrogen, and 24% for nitrogen. For air, nitrogen and helium, the local maximum are respectively 26%, 27% and 26%.

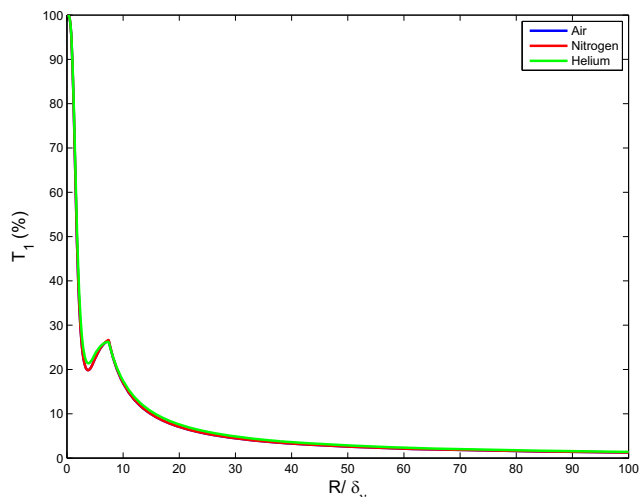


Figure 5:  $T_1$  in function of  $R/\delta_\nu$

The figure 6 represents  $T_2$  at the position  $y=0$  in function of  $R/\delta_\nu$  for air, nitrogen and azote. The curves have a similar form for the different type of gas. When  $R/\delta_\nu$  tends to zero,  $T_2$  tends to zero. When  $R/\delta_\nu$  tends to infinity,  $T_2$  tends respectively to 53%, 54% and to 48% for air, nitrogen and helium. Two specific values are observed for  $R/\delta_\nu = 3.1$  and  $7.4$ . For  $R/\delta_\nu = 3.1$ , the  $T_2$  reaches a local maximum of 50% for air, of 50% for nitrogen and of 45% for helium. For  $R/\delta_\nu = 7.4$ ,  $T_2$  is almost equal to zero for the three types of gas.

Figure 7 represents  $T_3$  at the position  $y=0$  in function of  $R/\delta_\nu$ . For the different types of gas, the curves have the same form. When  $R/\delta_\nu$  tends to zero,  $T_3$  tends to zero. When  $R/\delta_\nu$  tends to infinity,  $T_3$  converges to 38% for air, to 38% for nitrogen and to 41% for helium. For  $R/\delta_\nu = 7.4$ , the contribution reaches a local maximum. For air, nitrogen and helium, the local maxima

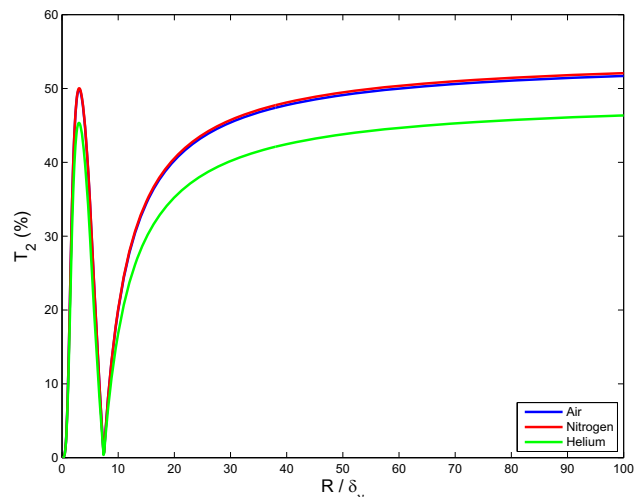


Figure 6:  $T_2$  in function of  $R/\delta_\nu$

are respectively 67%, 68% and 67%.

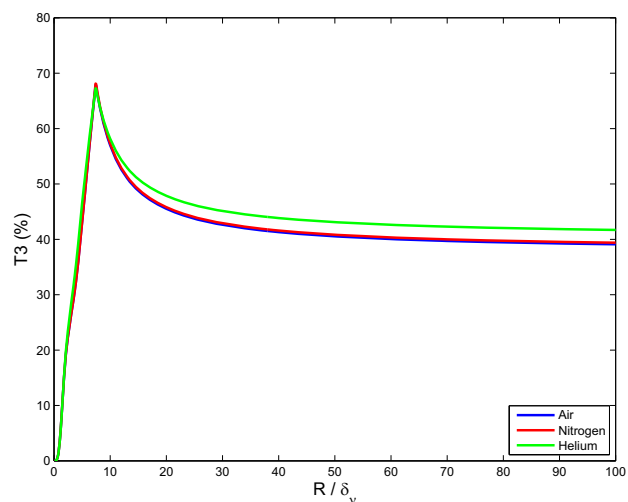


Figure 7:  $T_3$  in function of  $R/\delta_\nu$

Figure 8 represents  $T_4$  at the position  $y=0$  in function of  $R/\delta_\nu$  for air, nitrogen and azote. Whatever the type of gas, the curves have a similar form. When  $R/\delta_\nu$  tends to zero,  $T_4$  tends to zero. When  $R/\delta_\nu$  tends to infinity,  $T_4$  tends to 8% for air, to 7% for nitrogen and to 11% for helium. For  $R/\delta_\nu = 2.6$ , the contribution reaches a local maximum. The values of the local maximum are respectively 2%, 2% and 3% for air, nitrogen and helium. For  $R/\delta_\nu = 4.8$ ,  $T_4$  is almost equal to zero. At the same temperature, nitrogen has a viscosity less important than air wich has a viscosity less important than helium:

$$\mu_{\text{nitrogen}} < \mu_{\text{air}} < \mu_{\text{helium}} \tag{25}$$

For a standing wave, whatever the channel wide, it seems that the contribution increase with the viscosity of the fluid. In case of air, nitrogen and helium, the viscosity phenomenon has always a contribution less than 11% for standing wave. The viscosity can not be considered as the main cause of the acoustic streaming generation.

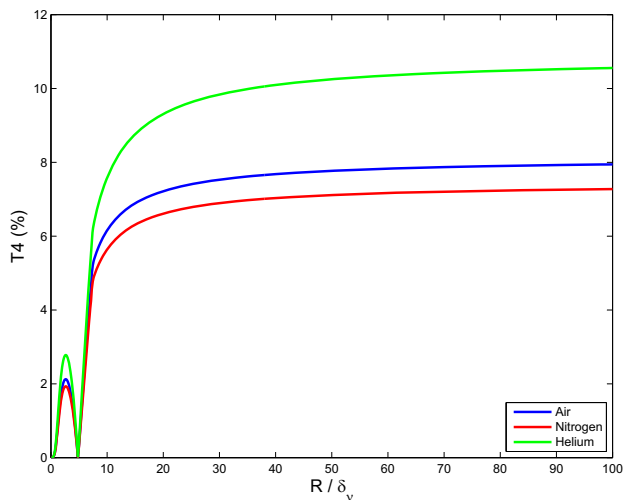


Figure 8:  $T_4$  in function of  $R/\delta_\nu$

## 5 Conclusion

The acoustic streaming has been investigated in the case of a standing wave. Measurements of the streaming velocity have been performed and compared with the theoretical values. As expected, the experimental values fit with the model. Three phenomena causing the acoustic streaming are identified: a mass flow, the Reynolds stress tensor and the viscous stress tensor. Their physical interpretations have been given and the contribution of each source to the axial streaming velocity has been quantified. For standing wave, the different contributions do not depend on the  $x$  coordinate. The influence of the duct thickness has been investigated. For narrow duct, the mass flow is the main contribution of the streaming velocity generation. For a wide channel, the Reynolds stress tensor contributes mainly to the streaming velocity generation. In case of air, nitrogen and helium, the viscosity phenomenon has always a contribution less than 11% for standing wave. The viscosity can not be considered as the main cause of the acoustic streaming generation. The investigation and the understanding of the streaming origin is a step to improve the energetic performance of thermoacoustic system.

## References

- [1] V. Gusev, S. Job, H. Bailliet, P. Lotton, M. Bruneau "Acoustic streaming in annular thermoacoustic prime-movers", J. Acoust. Soc. Am. **108**(3), 934-945 (2007)
- [2] G.W. Swift, D.L. Gardner, S. Backhaus, "Acoustic recovery of lost power in pulse tube refrigerators", J. Acoust. Soc. Am. **105**(2), 711-724 (1998)
- [3] J. Lighthill, "Acoustic streaming", Journal of Sound and Vibration, 391-418 (1978)
- [4] J.R. Olson, G.W. Swift, "Acoustic streaming in pulse tube refrigerators: tapered pulse tubes", Cryogenics **37**(12), 769-776 (1997)
- [5] H. Bailliet, V. Gusev, R. Raspet, R.A. Hiller, "Acoustic streaming in closed thermoacoustic devices", J. Acoust. Soc. Am. **110**(4), 1808-1821 (2001)
- [6] M.F. Hamilton, Y.A. Llinskii, E.A. Zabololotskaya, "Nonlinear two-dimensional model for thermoacoustic engines", J. Acoust. Soc. Am. **111**(5), 2076-2086 (2002)
- [7] S. Moreau, H. Bailliet, J.C. Valière, "Measurements of inner and outer streaming vortices in a standing waveguide using laser doppler velocimetry", J. Acoust. Soc. Am. **123**(2), 640-647 (2007)
- [8] W.P. Arnott, H.E. Bass, R. Raspet, "General formulation of thermoacoustics for stacks having arbitrarily shaped pore cross sections", J. Acoust. Soc. Am. **90**(6), 3228-3237 (1991)